



Original article

Structural, optical and photocatalytic activity of Ce³⁺ doped Co–Mg nanoparticles for wastewater treatment applications

N.M. Basfer*, Nuha Al-Harbi

Department of Physics, Faculty of Applied Sciences, Umm Al-Qura University, Makkah, Saudi Arabia

ARTICLE INFO

Article history:

Received 4 June 2022

Revised 3 August 2022

Accepted 6 November 2022

Available online 12 November 2022

ABSTRACT

Chemical effluent, particularly organic dyes, has become a major problem of our day because of its connection to carcinogenic health risks. Hence, rare earth element cerium (Ce) doped cobalt-magnesium ferrites were prepared with the formula $\text{Co}_{0.7}\text{Mg}_{0.3}\text{Ce}_x\text{Fe}_{2-x}\text{O}_4$ (labeled CMCF) by a combustion approach as an efficient nano-photocatalyst deliberated for disposal these pernicious dyes. The characterization tests for the CMCF nanoferrites were performed via XRD, STEM-EDS, and DR techniques. XRD results asserted the spinel single-phase formation for all the prepared CMCF ferrites. The lattice parameter and crystallite size of CMCF nanoferrites have abnormal behavior, which diminishes from 8.4077 to 8.3922 Å and 34.66 to 20.76 nm, respectively, despite the superseding process is a larger ion (Ce) instead of a smaller one (Fe). STEM images of the prepared nanoparticles are almost spherical crystallites with some agglomerations. The optical band gap of CMCF nanoparticles was tuned to be narrower by Ce³⁺ additions. Using the photocatalyst CMCF(x = 0.1), the MB's hue faded from blue to nearly colorless with an efficiency of 95.49 %, in 60 min. Three reasons why the CMCF(x = 0.1) photocatalyst gets the superior photocatalytic performance. Four steps were introduced to manifest the MB degradation mechanism utilizing the CMCF (x = 0.1) photocatalyst. The CMCF nanomaterials have significant prospects to be operated as promising photocatalysts for toxic MB disposal through wastewater treatment processes.

© 2022 The Author(s). Published by Elsevier B.V. on behalf of King Saud University. This is an open access article under the CC BY-NC-ND license (<http://creativecommons.org/licenses/by-nc-nd/4.0/>).

1. Introduction

Toxic contaminants, such as organic dyes, are released into the environment via the disposal of industrial effluent. Besides polluting water, dyes industrial effluent slows down photosynthesis in plants and animals, causing problems in aquatic ecosystems (Abdo et al., 2022). Many dyes are cancerous, have little biodegradability, and have a half-life of over two months under sunlight. It is thus of significant concern to the scientific world that dyes must be eliminated (Bessy et al., 2022). Especially the stable and non-biodegradable features of the methylene blue (MB) dye make them very hazardous to people and animals (Abdo et al., 2021). For preserving human and aquatic life, the appropriate removal of dye contaminants is critical. The photocatalysis technique is preferred because it is an efficient, affordable, and environmentally friendly

product (Kang et al., 2021; Li et al., 2021). Photocatalysts use solar energy in oxidation and reduction processes to decompose organic compounds. Semiconductor utilization in the photocatalysis process is fascinating topic for scientists because of its remarkable features (Kannan et al., 2020). Semiconductor spinel ferrites, as organic dye degradation photocatalysts, are gaining great attention from scientists due to their appropriate bandgap, non-toxicity, outstanding properties, and high photostability (Zhang et al., 2021). Particularly, cobalt ferrite (CoFe_2O_4), with its stability, visible light absorption capabilities, and lower band gap value, is an excellent choice for photocatalysis applications (Mmelesi et al., 2021). Also magnesium ferrite (MgFe_2O_4), with its large surface area, narrow band gap, and non-toxicity, is considered a promising adsorbent and photocatalyst (Kaur and Jeet 2022). Therefore, a ferrite system containing both CoFe_2O_4 and MgFe_2O_4 systems was chosen to produce a superior system for photocatalysis applications. The doping process is a frequently used procedure in nanoferrite materials, which includes introducing atoms or ions of desired elements to enhance their performance or properties (Mansour et al., 2021a; Abdo and Sadeq, 2021; Ali et al., 2021; Mansour et al., 2021d; Ahmed et al., 2013; Ahmed et al., 2011). Rare earth (RE) elements, as La, Sm, Ce, etc., are major kind of dopants with oxidation states ($3+$) and ($4+$), which directly influence the properties of ferrites

* Corresponding author.

E-mail address: noorbasfer20@gmail.com (N.M. Basfer).

Peer review under responsibility of King Saud University.



Production and hosting by Elsevier

via their f-electronic arrangement that confers unique physical features. Padalia et al. reported that RE elements with 3 + state is the most stable elements (Padalia et al., 2016). Meanwhile, cerium (Ce) is a striking RE element with a stable 4 + state with electronic orders $4f^0$, $5d^0$, $6s^0$. Irfan et al. investigated photocatalytic activity for methylene orange dye degradation utilizing Ce ions doped Co-Cd nanoferrite system, which was nearly 50 % in 60 min and 98 % in 180 min (Irfan et al., 2022). Meena et al. reported that the photocatalytic efficiency of manganese ferrite was enhanced by Ce doped which reached 98 % for MB dye in 75 min (Meena et al., 2021). Many researchers have studied the impact of Ce^{3+} cations in enhancing the photocatalytic efficiency of various spinel systems as; copper (Nasrabadi et al., 2016) and nickel (Somanathan et al., 2019), and cobalt-nickel (Kousar et al., 2022) ferrites. Bearing these in mind, by choosing a new ferrite system, we overcame these ferrites' major limitations. Our new system is the cerium substituted cobalt-magnesium nanoferrite as a photocatalyst, with a smaller size and higher area, which is not yet reported.

Therefore, the following aspects are the main objectives of this study: (i) synthesis and characterization of Ce substituted Co-Mg nanoferrites with formula $Co_{0.7}Mg_{0.3}Ce_xFe_{2-x}O_4$ (labeled CMCF); (ii) investigating how best to incorporate cerium ions into a ferrite lattice; (iii) studying the Ce effect in tuning the band gap energy of CMCF nanoferrites; (iv) reporting the photocatalytic mechanism of CMCF in MB degradation; (v) investigation of photocatalytic efficiency of CMCF under solar simulator irradiation for MB removal for wastewater treatment.

2. Experimental techniques

The citrate combustion approach (Al-Bassami et al., 2020) has been utilized to prepare the new nanoferrites with the formula $Co_{0.7}Mg_{0.3}Ce_xFe_{2-x}O_4$ (CMCF) for $x = 0-0.1$; in which x steps by 0.02. The highly pure metal nitrates and citric acid were utilized and dissolved in a minimal deionized water quantity. Then were neutralized using ammonia for a pH value reaching exactly 7 (Mansour et al., 2017), and stirred by a magnetic stirrer and then heating at a temperature $t = 250$ °C. Before starting characterization procedures, all the prepared CMCF nanoferrites were ground by a gate mortar for an hour to obtain homogenous powders. The structural elucidation of CMCF nanoferrites was complemented using a powder X-ray diffractometer, Shimadzu XRD 6000, where the 2θ span within $10^\circ-80^\circ$ utilizing a radiation Cu-K α ($\lambda = 0.154$ 05 nm). FTIR spectra for all CMCF nanoferrites were performed in the frequency span of $200-4000$ cm^{-1} on a desktop FTIR model of "Bruker Tensor 27" spectrometer". The particles and shapes of the CMCF nanoferrites were defined using Carl Zeiss STEM model "Sigma 500VP microscope". At room temperature, we measured the diffuse reflectance (DR %) of all CMCF ferrite nanoparticles. The photocatalytic efficiency of CMCF nanoferrites was studied using a 350 W Xenon lamp. 10 mg CMCF powder, a 0.25L MB dye solution with a 5 ppm concentration, was used for the photocatalytic examination.

3. Results and discussion

3.1. XRD studies

Fig. 1 embodies the indexed XRD patterns of all CMCF ferrite samples. The XRD peaks indexing and sequence match those reported in JCPDS reference cards # 00-001-1121 and # 01-088-1943 for cobalt and magnesium ferrites, respectively. Hence, we made sure of the formation of spinel single-phase structure within all the prepared CMCF ferrites. No extra peaks for any constituents are observed, demonstrating that the crystalline spinel structure

spread out over CMCF materials without other phases. The XRD peaks width varied with other Ce^{3+} content, indicating that the surface to volume ratio modifies CMCF particles (Naik and Salker, 2012). The influence of Ce^{3+} addition on the unit cell dimensions of CMCF materials can be manifested in Fig. 2, exhibiting the 2θ values shifting of (3 1 1) peaks ($2\theta_{(311)}$) for different Ce^{3+} content. This figure obviously shows the gradual increase of $2\theta_{(311)}$ from 35.4097 to 35.4468° , with progressively lattice parameter (a_{exp}) decreased from 8.4077 to 8.3922 Å. All a_{exp} values of CMCF ferrites were calculated using the d_{hkl} spacing and hkl Miller indices via the equation $a_{exp} = d_{hkl} \sqrt{h^2 + k^2 + l^2}$ (Mansour et al., 2018a) and then listed in Table 1. Undoubtedly, this result of decreasing lattice parameter is completely unexpected where our superseding process is large cations Ce^{3+} (1.02 Å) instead of smaller ones Fe^{3+} (0.64 Å). This uncommon behavior of lattice parameter can be understood for the following reasons. The larger Ce^{3+} ions endeavor to expand the CMCF lattice, but microstrains have another active role, generating a restitution role to prevent this expansion. Obviously, the produced microstrains are larger than the expansion endeavors; hence, the CMCF lattice parameter decreases gradually. Moreover, the bond dissociation energy (E_{BD}) of the Ce-O bond is 795 kJ/mol at 298 K, and the E_{BD} of the Fe-O bond is 409 kJ/mol. Therefore Ce-O is potent and short, leading to curtailment of CMCF lattice volume and their parameter (Dasent, 1982), see Fig. 2. The crystallite size (D) and internal strain (ϵ_i) of our CMCF ferrites were calculated utilizing Williamson-Hall (W-H) approach by analyzing the XRD peak broadening, by the following equation (Mansour et al., 2020).

$$\beta \cos \theta = \frac{k\lambda}{D} + 4\epsilon_i \sin \theta$$

All W-H plots ($\beta \cos \theta$ versus $4\epsilon_i \sin \theta$) are manifested in Fig. 3a-f. From W-H plots, D and ϵ_i values are calculated from $D = (k\lambda / \text{intercepts})$ and $\epsilon_i = \text{slope of the fitted lines}$, where k is a constant (0.9) and λ is X-ray wavelength. All D and ϵ_i values are collected in Table 1, demonstrating that D values are in the nanometric range, which diminishes gradually from 34.66 to 20.76 nm with Ce/Fe superseding process. As mentioned above, this is a logical result for the EBD values disparity of Ce-O, and Fe-O bonds. Therefore more energy is requisite to force Ce^{3+} ions merge into the CMCF lattice and produce $Ce^{3+}-O^{2-}$ bonds. Consequently, our superseding process (Ce/Fe) results interior lattice stress, which prevents CMCF lattice growth and decreases their size. Hence, CMCF nanoferrites have higher thermal stability than the pristine $Co_{0.7}Mg_{0.3}Fe_2O_4$ sample where extra energy is requisite for crystallization process (Thankachan et al., 2013). Mansour et al. reported a similar result for decreasing crystallite size by doping larger ions lanthanum at the expense of iron ions (Mansour et al., 2021b). All ϵ_i values are positive, demonstrating that the CMCF nanoferrites have tensile strain (Mansour et al., 2019), which is a logical result for Ce/Fe superseding process.

Additional calculations were made to determine the X-ray density (d_{XRD}) (Mansour et al., 2018b) through the equation $d_{XRD} = \frac{ZM}{a^3 N_A}$, where Z is the number of molecules per unit cell, M is the molecular weight of the sample (g/mole), N_A is the Avogadro's number (6.023×10^{23} atom/mole). The specific surface area of all the samples was determined by the formula $S = \frac{6000}{D \times d_{XRD}}$ (Chahar et al., 2021). All these parameters were tabulated in Table 1. An increasing trend for d_{XRD} values is obtained, which is a logical result for the superseding process of Ce/Fe cations, where Ce has a molecular weight of 140.116 g/mol, and Fe has 55.85 g/mol. With additional Ce^{3+} content, S values exhibit an increment behavior, a natural conclusion of the decrementing behavior for crystallite size; See Table 1. Therefore our CMCF nanoferrites are more appropriate for provid-

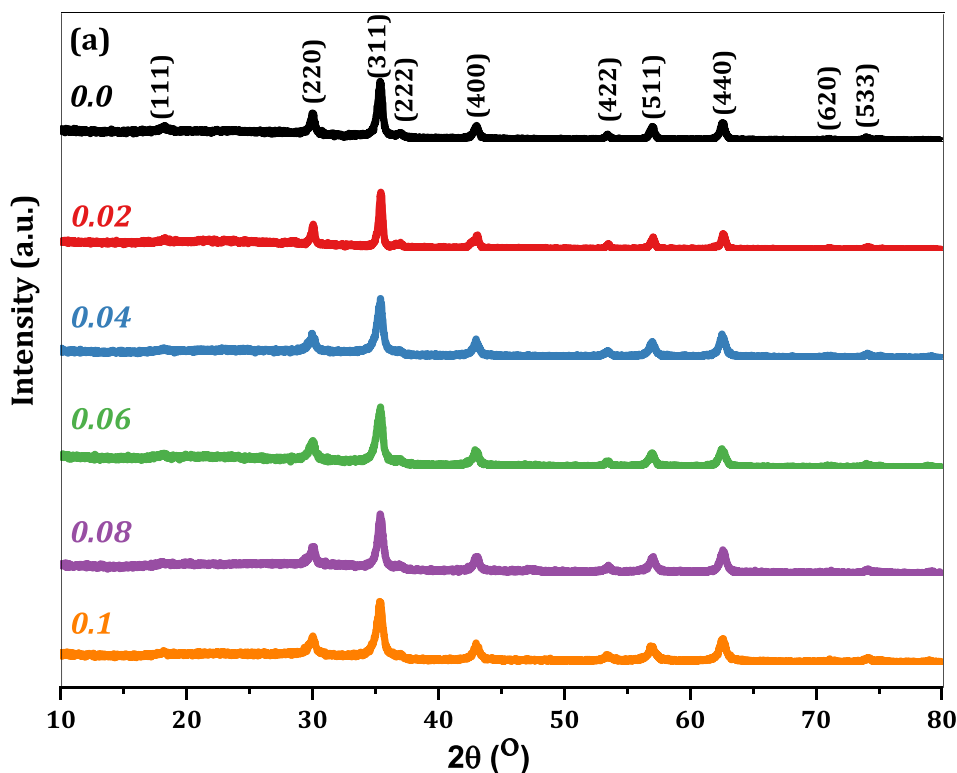


Fig. 1. XRD diffractograms of $\text{Co}_{0.7}\text{Mg}_{0.3}\text{Ce}_x\text{Fe}_{2-x}\text{O}_4$; $x = 0.0$, $x = 0.02$, $x = 0.04$, $x = 0.06$, $x = 0.08$ and $x = 0.1$ nanoferrites.

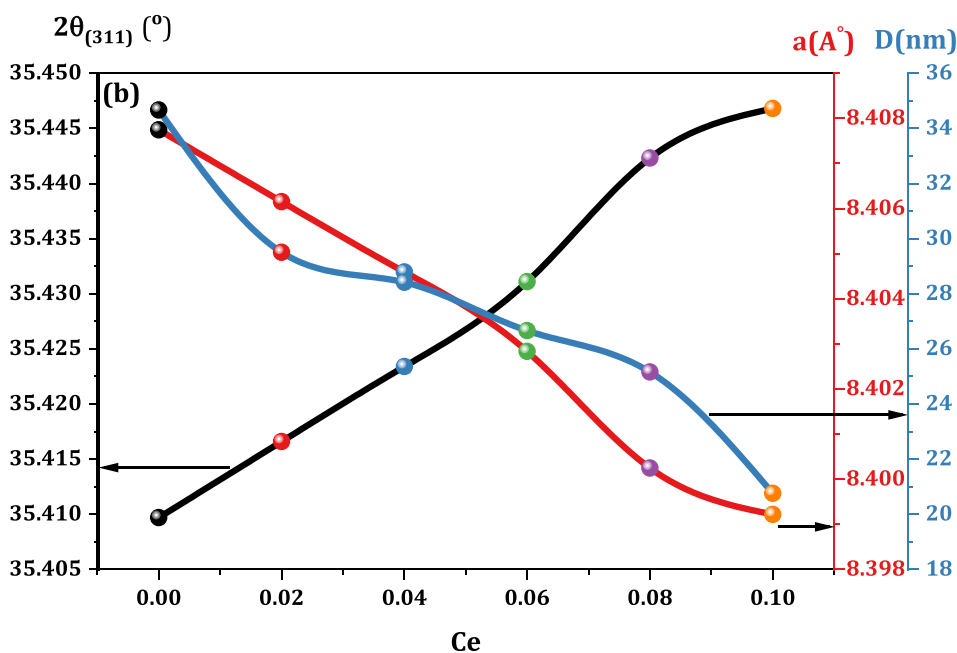


Fig. 2. Dependence of 2θ values shifting of (311) peaks ($2\theta_{(311)}$), lattice parameter (a) and crystallite size (D) of CMCF nanoferrites on Ce content.

ing a large surface area which is most required for absorption in photocatalysis applications, as seen later.

3.2. Electron microscopy analysis:

Fig. 4a-f shows the STEM-EDX images of $\text{Co}_{0.7}\text{Mg}_{0.3}\text{Ce}_x\text{Fe}_{2-x}\text{O}_4$, ($x = 0.0, 0.04$ and 0.1) samples; as models for all CMCF nanoferrites. Fig. 4a-c manifests the STEM images for the selected samples,

which confirm the nanocrystalline nature of the CMCF nanoparticles (Abdo, El-Daly, 2021). These nanoparticles are almost spherical crystallites with some agglomerations produced from the magnetic properties of the CMCF ferrites and their surface binding forces. To scrutinize the CMCF nanoparticle constituents' cations, EDX micrographs are collected for the elected nanoferrites. Fig. 4d-f shows the EDX charts of $\text{Co}_{0.7}\text{Mg}_{0.3}\text{Ce}_x\text{Fe}_{2-x}\text{O}_4$, ($x = 0.0, 0.04$ and 0.08). The EDX micrographs revealed the entity of all CMCF con-

Table 1
The lattice parameter a_{exp} , crystallite size D, lattice strain ϵ_i , X-ray density d_{XRD} , specific surface area S, and optical bandgap E_g , of CMCF nanoferrites.

x	a_{exp} (Å)	D (nm)	ϵ_i	d_{XRD} ($g.cm^{-3}$)	$S \times 10^8$ (cm^2/g)	E_g (eV)
0.0	8.4077	34.66	6.03E-4	5.012	3.46	1.55
0.02	8.4062	29.51	0.00114	5.052	4.03	1.54
0.04	8.4046	28.41	7.81E-4	5.093	4.15	1.57
0.06	8.4028	26.66	3.53E-4	5.134	4.38	1.54
0.08	8.4003	25.16	6.03E-4	5.176	4.61	1.54
0.1	8.3992	20.76	0.00116	5.216	5.54	1.53

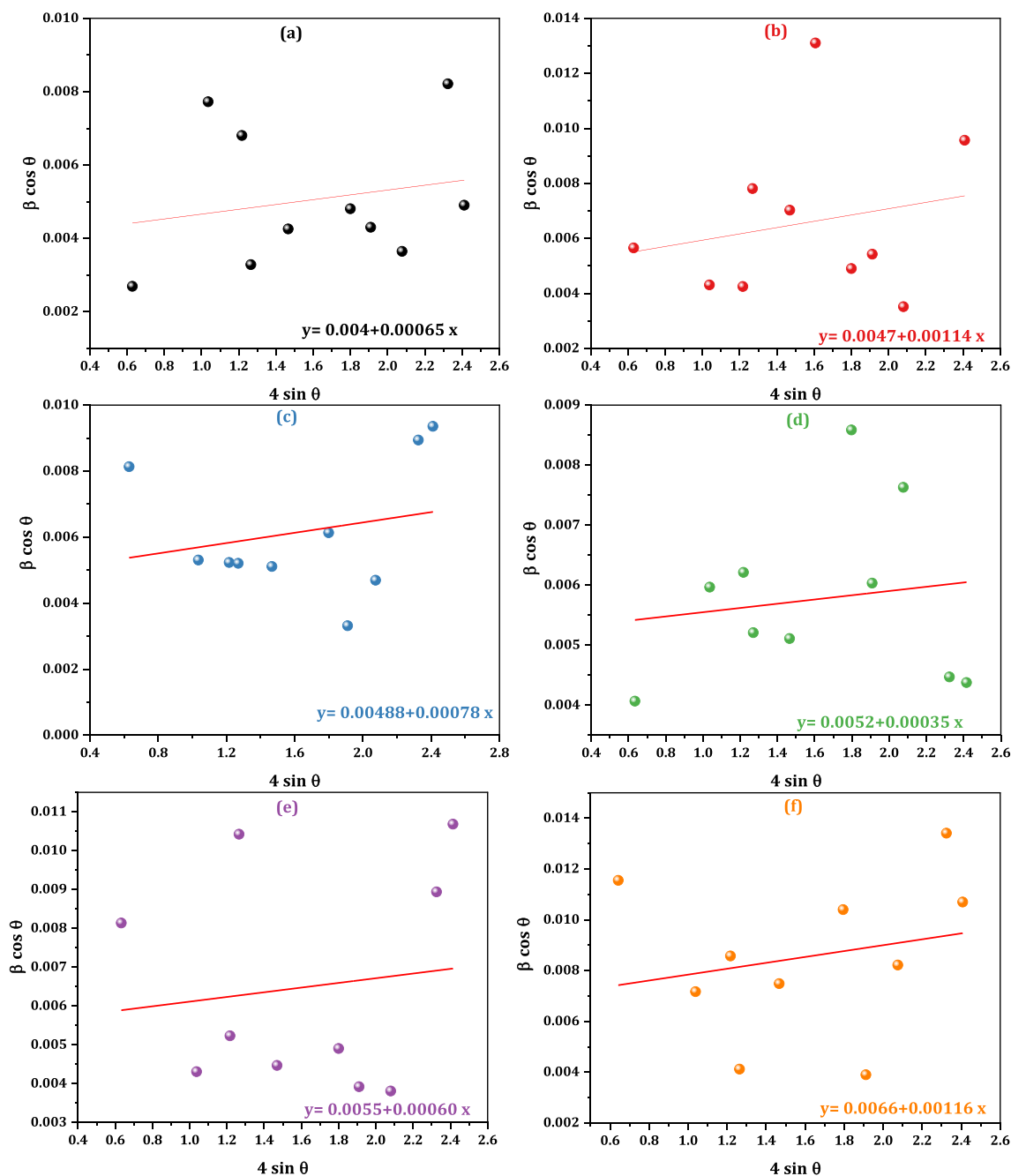


Fig. 3. a–f: W–H plots of $Co_{0.7}Mg_{0.3}Ce_xFe_{2-x}O_4$; $x = 0.0$, $x = 0.02$, $x = 0.04$, $x = 0.06$, $x = 0.08$ and $x = 0.1$ nanoferrites.

stituents' ions only; Co, Mg, Ce, Fe, and O; confirming that our samples are pure CMCF powders without any unknown elements.

These figures also show the increment of Ce quantity on account of Fe ones is nearly identical to Ce/(Ce + Fe) percentage through

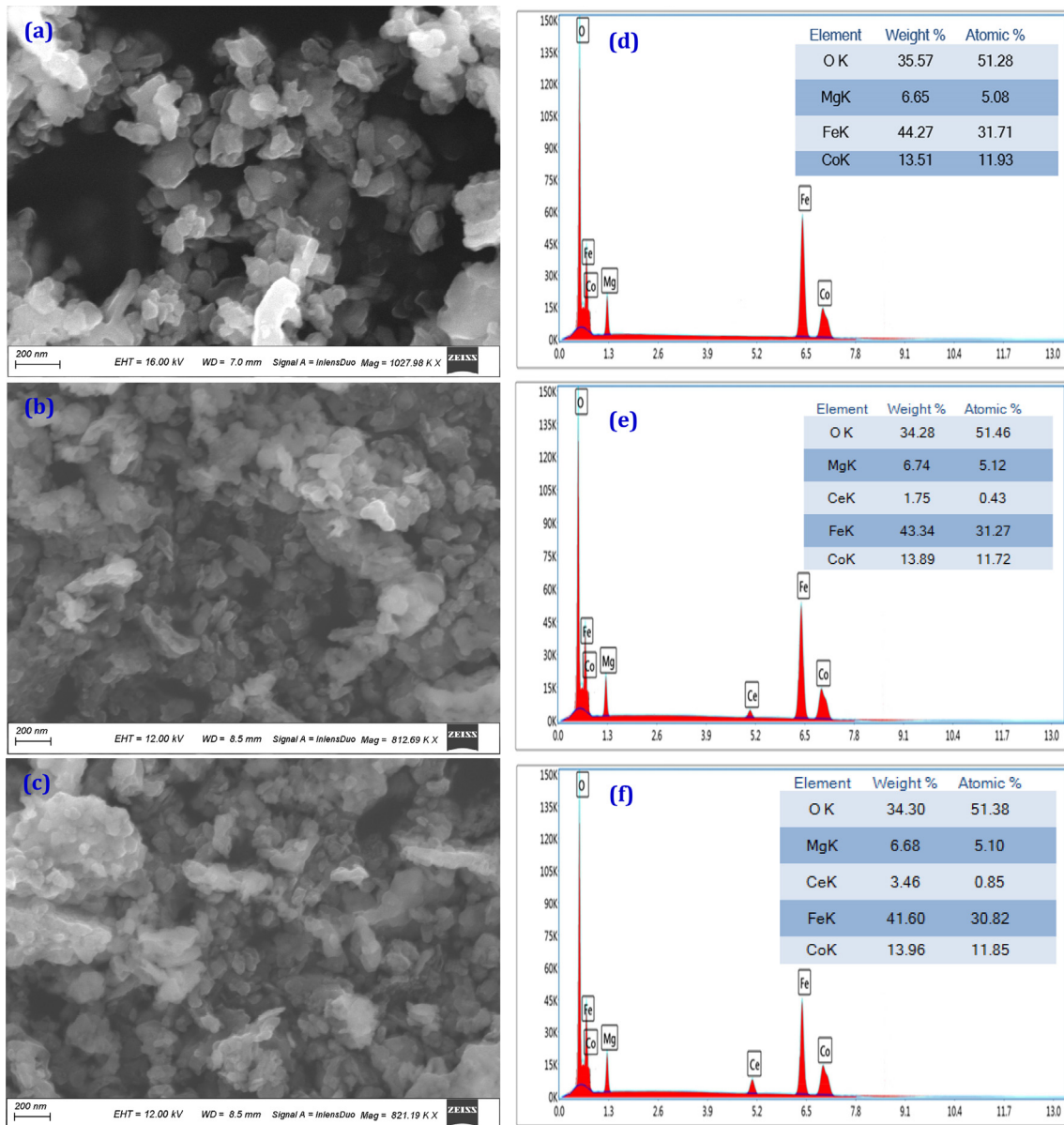


Fig. 4. A-f: stem-eds micrographs of (a) $\text{Co}_{0.7}\text{Mg}_{0.3}\text{Fe}_2\text{O}_4$, (b) $\text{Co}_{0.7}\text{Mg}_{0.3}\text{Ce}_{0.04}\text{Fe}_{1.96}\text{O}_4$ and (c) $\text{Co}_{0.7}\text{Mg}_{0.3}\text{Ce}_{0.08}\text{Fe}_{1.92}\text{O}_4$ ferrite nanoparticles.

the preparation process. The ratios $(\text{Co} + \text{Mg})/\text{Fe}$ in the pristine sample, and $(\text{Co} + \text{Mg})/(\text{Ce} + \text{Fe})$, in nanoferrites containing Ce^{3+} ions, are almost 0.5, demonstrating the CMCF nanoferrites' pureness.

3.3. Optical studies

3.3.1. DR spectroscopy of CMCF nanoferrites and their optical energy gap

Diffuse reflectance spectroscopy is used to assess the optical characteristics of the studied CMCF nanoferrites. The reflectance function $F(R)$ of a suitably thick layer may be estimated utilizing Kubelka and Munk (K-M) model (Alahmari et al., 2022).

$$F(R) = \frac{(1 - R)^2}{2R}$$

The CMCF nanoferrites' energy band gap (E_g) values may well be estimated using Tauc's equation (Alahmari et al., 2022) as follows:

$$[F(R_{\infty}) \cdot h\nu]^{\frac{1}{n}} = A(h\nu - E_g)$$

The exponent n specifies the transition kind, whether direct ($\frac{1}{2}$) or indirect (2) allowed kinds. It is clear from Fig. 5a-f that the direct band gaps in our CCZY nanoferrites are applicable. When Tauc's plots converge at $y = 0$, E_g will be accurately calculated in the eV unit. It is shown in Table 1 that the CMCF nanoferrites have an outstanding E_g demeanor. A sample with $x = 0.0$ has an E_g value of 1.55 eV. By increasing the Ce^{3+} concentration from $x = 0.02$ to $x = 0.1$, the CMCF nanoferrites had lower E_g values of 1.54, 1.57, 1.54, 1.55, and 1.53 eV. Because of this, the $\text{Co}_{0.7}\text{Mg}_{0.3}\text{Fe}_2\text{O}_4$ band gap may be tuned to be ideal candidates for proper activities that fall within the semiconductor band gap range. The inverse correlation between E_g and crystallite size (Mansour et al., 2021c) justifies the behavior of E_g , which is based on the behavior of crystallite size. As far as we know, this study was the first to investigate the optical band gaps of $\text{Co}_{0.7}\text{Mg}_{0.3}\text{Ce}_x\text{Fe}_{2-x}\text{O}_4$ nanoparticles.

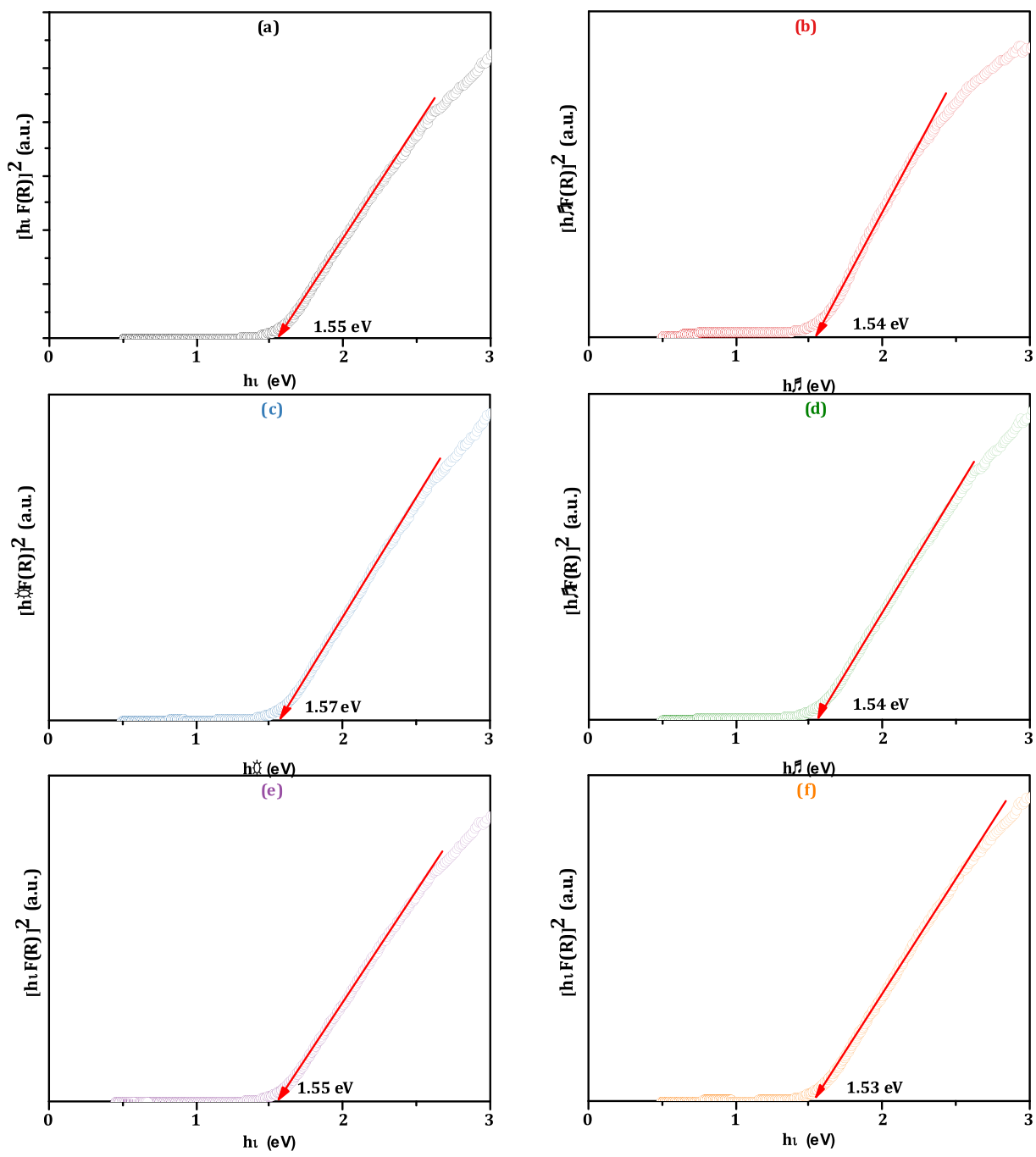


Fig. 5. A-f: $[hvF(R)]^2$ versus photon energy (hv) graphs of CMCF nanoferrites (a linear regression to the hv axis gives the E_g of the corresponding nanoferrite).

3.3.2. Photocatalytic analyses

The photodegradation procedure employing nanoferrites is an attractive way to erode organic dyes into secure yields, H_2O and CO_2 , by sunlight (Li et al., 2022). The bandgap of our CMCF nanoparticles reduces slowly by cerium ions addition, revealing that our nanoparticles may be operated like usable visible-light-driven efficient photocatalyst. Accordingly, the catalytic analysis of our CMCF nanoferrites is evaluated concerning a toxic organic dye, methylene blue (MB). The significance of such analysis is probing the CMCF nanoferrites utilization in wastewater treatment. The importance of operating the CMCF nanoferrites, like whole spinel nanoferrites, is long-lasting, reused several periods, have a lower expense and have a thinner bandgap. Many new results (Shakil et al., 2022; Vinosha et al., 2022, Mansour et al.,

2020) appraised efficacious outcomes for photocatalytic processes based on the RE element, nanoferrite band gap values besides their nanometric size. It is attended that the CMCF($x = 0.1$) nanoferrite acquires the most increased photocatalytic efficiency based on their highest Ce^{3+} ions, miniature E_g , and teeny dimension values. So, this nanoferrite is expected to produce a remarkable result for MB degradation. Some CMCF nanoferrites are preferred to probe their photocatalytic response using MB; the nanoferrite with $x = 0.0$ (pure specimen), $x = 0.04$ (with the moderate value of Ce^{3+} and highest E_g), and $x = 0.1$ (highest Ce^{3+} value, lower E_g and lower size values). A solar simulator instrument was utilized to irradiate pure MB dye, and our chosen CMCF nanoferrites via a Xenon arc lamb 350 W. MB solution (0.25 L and 5 ppm) was employed with 10 mg from CMCF samples for the degradation examination. Fig. 6-

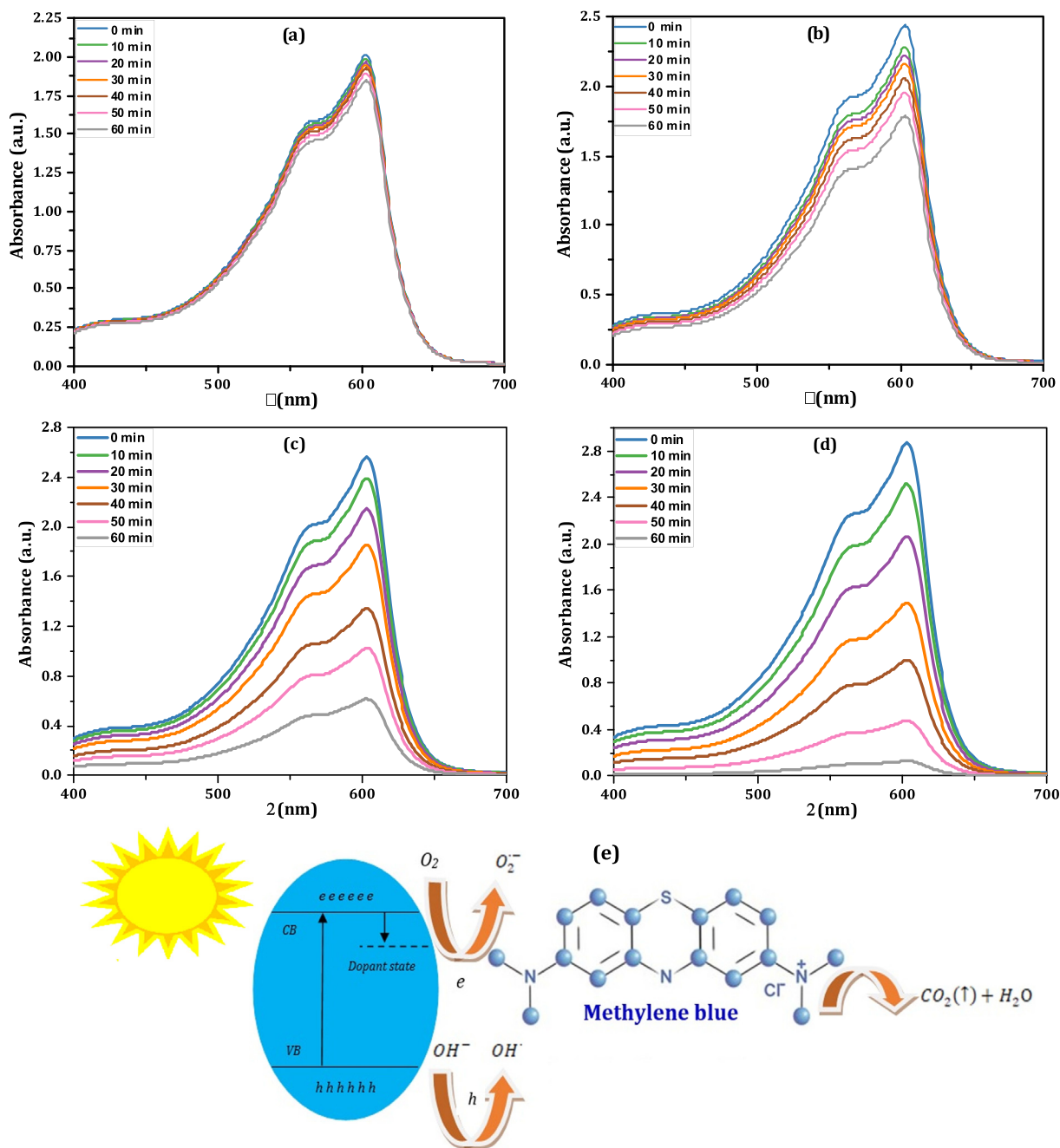


Fig. 6. A-e: uv-vis. absorption spectra of mb, mb + CMCF(x = 0.0), MB + CMCF(x = 0.04) and MB + CMCF(x = 0.1) solutions measured at different exposure periods (0–60 min).

a-d manifests the absorption graphs of pure MB, MB + CMCF(x = 0.0), MB + CMCF(x = 0.04) and MB + CMCF(x = 0.1) collected regularly with time at (0, 10, 20, 30, 40, 50 and 60 min). In all the curves, there is a peak of nearly 600 nm with a 563 nm shoulder, indicating the MB presence. There are no red or blue shifts in our solution's photocatalytic chemical processes as the exposure duration increases from t = 0 to 60 min. This situation implies that our solutions contain only pure photocatalytic chemical reactions. After exposure to the light for 60 min, the MB's hue faded from blue to colorless. The equivalent formula in Ref. (Zheng et al., 2022) has been used to assess the samples' degradation efficacy. Indeed, the sample CMCF(x = 0.1) had the maximum degrading efficiency in MB, with a 95.49 % degradation rate after 60 min of exposure. This is a noteworthy finding compared with the remainder specimens; 8.21 % for solely MB, 26.73 % for CMCF(x = 0.0) and

74.94 % for CMCF(x = 0.04). Apparently, Fig. 7a demonstrates the photodegradation efficiency for pure MB and MB employing CMCF(x = 0.0), CMCF (0.04) and CMCF (0.1) samples (as catalyst). Hence, our CMCF powders have been shown to improve MB degrading efficiency. It was reported that MB dye has a maximum degradation efficiency of 80 % after 240 min utilizing a cobalt magnesium ferrite system (Dojcinovic et al., 2021). Also, another research group declared that MB dye acquired a maximum efficiency of 77 % after 60 min via a cobalt zinc ferrite system (Deepika et al., 2021). Geetha et al. declared degradation efficiency for MB utilizing Ce substituted magnesium nanoferrites (MgCe_{0.1}Fe_{1.9}O₄) to be 82.69 % in 90 min (Geetha et al., 2021). Consequently, the degradation efficiency of the CMCF(x = 0.1) sample is an outstanding outcome (95.49 % at 60 min) compared with the literature review for MB removals. The reasons behind the sample CMCF

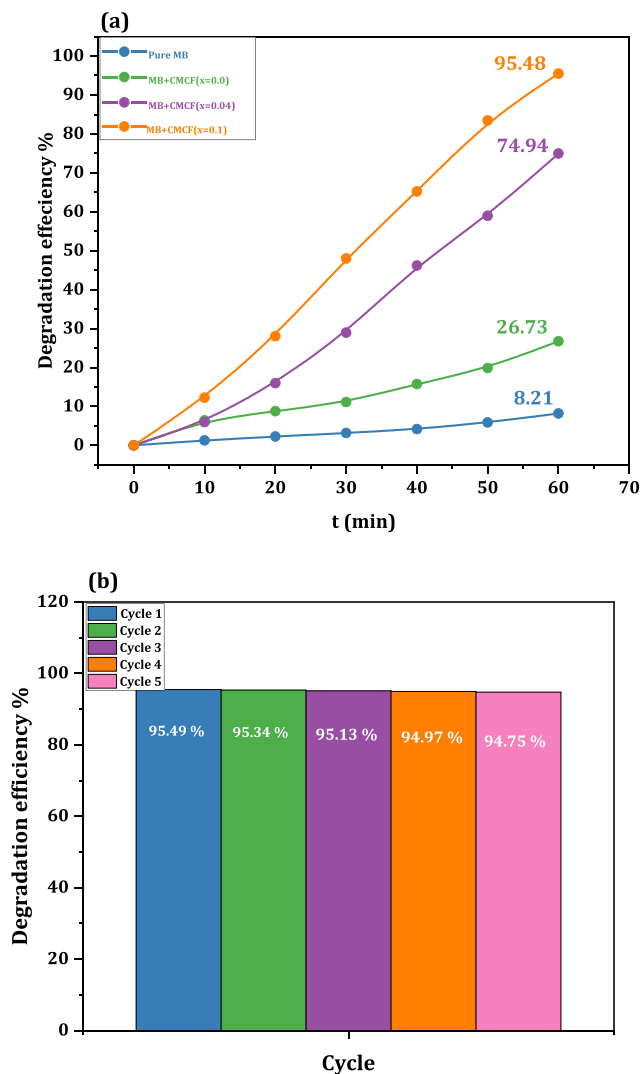


Fig. 7. A,b: (a) degradation efficiency for pure mb and mb with cmcf(x = 0.0), CMCF (x = 0.08) and CMCF (x = 0.1) samples, respectively (as catalysts) and (b) Recyclability of CMCF (x = 0.1) for the MB dye degradation up to 5 catalytic runs.

(x = 0.1) having the maximum efficiency are represented as follows:

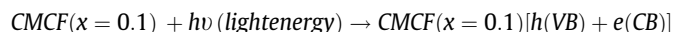
It has a smaller size, 20.76 nm, and hence has a larger surface area, see Table 1, which is preferable for the catalysis process. It has a lower E_g value, 1.53 eV, and thus enhances the excitations of electrons from the valence band (VB) into the conduction band (CB).

Cerium ions can operate as an electronic trapping center as a reminder of rare earth elements, which may slow the rate of e-h recombination.

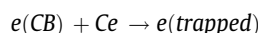
3.3.3. Degradation mechanism

Based on the semiconductor photocatalysis concept, rare earth ferrite valence electrons are driven by 350–750 nm irradiation light to create a very active light hole-electron pair that increases its visible-light catalytic performance. The nanoferrite CMCF (x = 0.1) will utilize, as a model, to discuss the MB degradation mechanism. The likely photodegradation pathway for MB employing the CMCF(x = 0.1) nanoferrite is illustrated in Fig. 6e, which can summarize the following steps. Abdo et al reported a similar mechanism for MB dye degradation (Abdo et al. 2021).

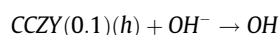
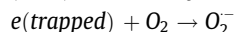
Step 1: The CMCF(x = 0.1) nanoferrite absorbs the incoming energy (hν), happens electrons (e) excitation from CMCF(x = 0.1) VB to their CB while departing holes (h) inside this VB.



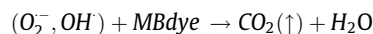
Step 2: Cerium ions work as electron capturing centers that capture the excited electrons leading to hindrance to the e-h pair combination.



Step 3: These electrons (trapped) transported from cerium ions combine with O₂ and generate superoxide radical (O₂⁻). While, h, generated in the VB of CMCF (x = 0.1), can get combined with (OH⁻) to create hydroxyl radical (OH[·]).



Step 4: The produced free radicals (O₂⁻ and OH[·]) led to MB degradation into natural and harmless components (CO₂(↑) + H₂O) (Kumar and Chand, 2022).



3.3.4. The CMCF photocatalysts recyclability

Nanoferrites recyclability is of major significance because of its ability to degrade the contaminants released by dyeing pollution. An external magnet can readily extract ferrites from the reaction mixture. After 60 min, the powders were detached and dried at RT. The recovered powders were transported to a quartz cuvette with fresh MB solution for the next cycle. This process was performed in 5 runs under similar conditions. The stability of the as-synthesized CMCF photocatalysts is that they did not exhibit any appreciable loss even after five cycles. The MB degradation in the presence of the nanoferrite CMCF(x = 0.1) for 5 subsequent cycles is represented in Fig. 7b, which shows no significant loss after these cycles. From Fig. 7b, the MB degradation efficiencies are 95.49 %, 95.34 %, 95.13 %, 94.97 %, and 94.75 %, respectively, with our CMCF photocatalyst, demonstrating their application in dye degradation and wastewater treatment.

3.3.5. Reaction kinetic studies

To identify the catalytic activity behavior of our CMCF nanoferrites, the three kinetic orders (0th, 1st and 2nd) were computed by the following relations (Aref et al., 2020).

$$A_t = A_0 - k_0 t, A_t = A_0 e^{-k_1 t}, \frac{1}{A_t} = \frac{1}{A_0} + k_2 t$$

Wherein A_t and A₀ represent absorbance after and before light irradiation. Fig. 8a-c manifest the A_t, ln(A₀/A_t) and 1/A_t versus time graphs for pure MB and (MB + CMCF nanoferrites (x = 0.0, 0.04, and 0.1). The k₀, k₁, and k₂ represent the three kinetic rate constants of 0th, 1st, and 2nd kinetics of MB and (MB + CMCF nanoferrites (x = 0.0 and 0.1) are determined then listed in Table 2. Table 2 also includes correlation coefficients (R²) for each case. For all the samples pure MB and (MB + CMCF nanoferrites (x = 0.0, 0.04 and 0.1), the zero-order is very convenient for the catalytic behavior, where its R² values are equal to 0.970, 0.975, 0.984 and 0.996 respectively, which are the maximum among all models.

4. Conclusion:

A facile, citrate combustion approach was utilized to prepare a new nanoferrite system of Co_{0.7}Mn_{0.3}Ce_xFe_{2-x}O₄ (CMCF); x = 0.0–0.1. XRD results demonstrated the formation of spinel single-phase structure within all the prepared CMCF ferrites, with no extra peaks for any constituents. Crystallite size values of all CMCF

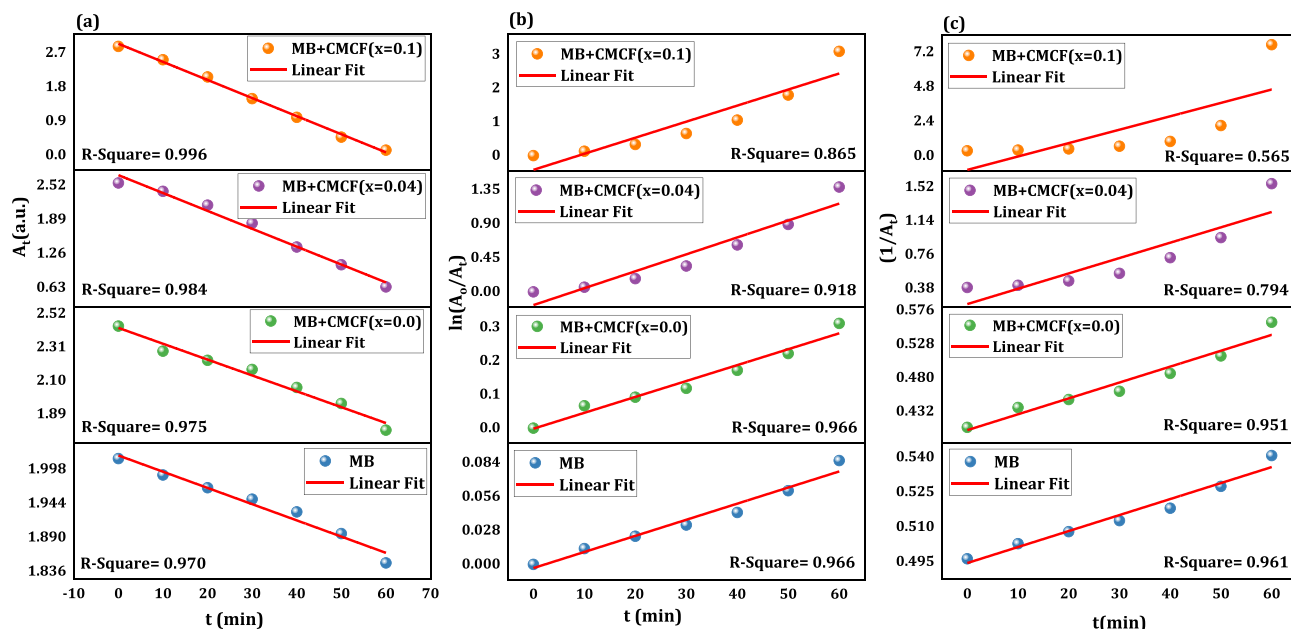


Fig. 8. A-c: the plots of (a) A_t , (b) $\ln(A_0/A_t)$ and (c) $1/A_t$ versus time along with their linear fits for mb dye without and with cmcf nanoparticles as photocatalysts.

Table 2

The kinetic rate constants (k_0 , k_1 and k_2) and correlation coefficient (R^2) for zeroth, first and second order reaction kinetics of MB dye with and without CMCF photocatalyst nanoparticles.

Sample	Kinetic model parameters		
	Zeroth order	first order	second order
Pure MB	$k_0 = 0.00257$ $R^2 = 0.970$	$k_0 = 0.00133$ $R^2 = 0.966$	$k_0 = 0.49449$ $R^2 = 0.961$
MB + CMCF(x = 0.0)	$k_0 = 0.00995$ $R^2 = 0.975$	$k_0 = 0.00473$ $R^2 = 0.966$	$k_0 = 0.40553$ $R^2 = 0.951$
MB + CMCF(x = 0.04)	$k_0 = 0.03307$ $R^2 = 0.984$	$k_0 = 0.02235$ $R^2 = 0.918$	$k_0 = 0.020363$ $R^2 = 0.7984$
MB + CMCF(x = 0.1)	$k_0 = 0.0478$ $R^2 = 0.996$	$k_0 = 0.04771$ $R^2 = 0.865$	$k_0 = 0.009303$ $R^2 = 0.565$

nanoferrites are in the nanometric range with decreasing behavior from 34.66 to 20.76 nm. All lattice strain values are positive, demonstrating that the CMCF nanoferrites have tensile strain. FTIR transmittance spectra of the CMCF ferrite powders revealed their distinct functional groups of tetrahedral and octahedral coordination. The EDX micrographs revealed the entity of all CMCF constituents' ions only; Co, Mg, Ce, Fe, and O, confirming the purity of our powders. The bandgap of all CMCF nanoferrites was tuned by Ce^{3+} additions and fell within the semiconductor bandgap range. The nanoferrite CMCF(x = 0.1) had the maximum degrading efficiency in MB, with a 95.49% degradation rate after 60 min compared with the remainder specimens; 8.21% for solely MB, 26.73% for CMCF(x = 0.0) and 74.94% for CMCF(x = 0.04). The likely photodegradation pathway for MB employing the CMCF(x = 0.1) nanoferrite may be grasped through four steps. The MB degradation using the nanoferrite CMCF(x = 0.1) after 5 subsequent cycles showed no significant. The zero-order model is the most convenient one for identifying photocatalytic behavior. The nanoferrite $Co_{0.7}Mg_{0.3}Ce_{0.1}Fe_{1.9}O_4$ can be utilized as a photocatalyst for MB effluents removal with an efficiency of 95.49% in just an hour.

Declaration of Competing Interest

The authors declare that they have no known competing financial interests or personal relationships that could have appeared to influence the work reported in this paper.

Appendix A. Supplementary material

Supplementary data to this article can be found online at <https://doi.org/10.1016/j.jksus.2022.102436>.

References

- Abdo, M.A., El-Daly, A.A., 2021. Sm-substituted copper-cobalt ferrite nanoparticles: Preparation and assessment of structural, magnetic and photocatalytic properties for wastewater treatment applications. *J. Alloys Compd.* 883, 160796.
- Abdo, M.A., Sadeq, M.S., 2021. Covalency and Racah parameters of Fe^{3+} in Mn–Zn–Cr nanoferrites. *Ceram. Int.* 47, 28237–28239.
- Abdo, M.A., Mansour, S.F., Al-Bassami, N.S., Abu-Elsaad, N.I., 2022. Yttrium substituted Co–Cu–Zn nanoferrite: A synergetic impact of Y^{3+} on enhanced physical properties and photocatalysis. *Ceramics International* 48 (11), 15314–15326.
- Ahmed, M.A., Mansour, S.F., Abdo, M.A., 2011. Characterization and dramatic variations of the magnetic properties of Cu-doped nanometric Co ferrite. *Phys. Scr.* 84, 055602. <https://doi.org/10.1088/0031-8949/84/05/055602>.
- Ahmed, M.A., Mansour, S.F., Abdo, M.A., 2013. Improvement of the physical properties of novel (1-y) $Co_{0.8}Cu_{0.2}Fe_2O_4$ + (y) $SrTiO_3$ nanocomposite. *Mater. Res. Bull.* 48. <https://doi.org/10.1016/j.materresbull.2013.01.034>.
- Al-Bassami, N.S., Mansour, S.F., Abdo, M.A., 2020. The magneto-mechanical properties of cobalt substituted Mg–Zn nanoferrites. *J. Supercond. Nov. Magn.* 33 (10), 3077–3086.
- Ali, T.M., Ismail, S.M., Mansour, S.F., Abdo, M.A., Yehia, M., 2021. Physical properties of Al-doped cobalt nanoferrite prepared by citrate–nitrate auto combustion method. *J. Mater. Sci.: Mater. Electron.* 32 (3), 3092–3103.
- Bessy, T.C., Bindhu, M.R., Johnson, J., Chen, S.M., Chen, T.W., AlMaary, K.S., 2022. UV light assisted photocatalytic degradation of textile waste water by $Mg_{0.8-x}Zn_xFe_2O_4$ synthesized by combustion method and in-vitro antimicrobial activities. *Environ. Res.* 204, 111917.
- Chahar, D., Taneja, S., Bisht, S., Kesarwani, S., Thakur, P., Thakur, A., Sharma, P.B., 2021. Photocatalytic activity of cobalt substituted zinc ferrite for the degradation of methylene blue dye under visible light irradiation. *J. Alloys Compd.* 851, 156878.
- Dasent, W.E., 1982. *Inorganic Energetics: An Introduction*. Cambridge University Press.
- Dojcinovic, M.P., Vasiljevic, Z.Z., Pavlovic, V.P., Barisic, D., Pajic, D., Tadic, N.B., Nikolic, M.V., 2021. Mixed Mg–Co spinel ferrites: Structure, morphology, magnetic and photocatalytic properties. *J. Alloys Compd.* 855, 157429.
- Geetha, K., Udhayakumar, R., Manikandan, A., 2021. Enhanced magnetic and photocatalytic characteristics of cerium substituted spinel $MgFe_2O_4$ ferrite nanoparticles. *Phys. B: Condens. Matter.* 615, 413083.
- Irfan, M., Ayyaz, M., Naz, M.Y., Shukrullah, S., Munir, M.M., Kamran, K., et al., 2022. Testing of optical, dielectric and photocatalytic properties of Ce^{3+} doped cobalt–cadmium nanocomposite for high frequency devices and wastewater treatment. *Ceram. Int.* 48 (6), 8517–8528.
- Kang, J., Tang, Y., Wang, M., Jin, C., Liu, J., Li, S., et al., 2021. The enhanced peroxymonosulfate-assisted photocatalytic degradation of tetracycline under visible light by g- C_3N_4 /Na– $BiVO_4$ heterojunction catalyst and its mechanism. *Journal of Environmental Chemical Engineering* 9, (4) 105524.

- Kannan, K., Radhika, D., Sadasivuni, K.K., Reddy, K.R., Raghu, A.V., 2020. Nanostructured metal oxides and its hybrids for photocatalytic and biomedical applications. *Adv. Colloid Interface Sci.* 281, 102178.
- Kaur, M., Jeet, K., 2022. Mechanistic insight into adsorption and photocatalytic potential of magnesium ferrite-bentonite nanocomposite. *J. Photochem. Photobiol. A: Chem.* 425, 113717.
- Kousar, T., Aadil, M., Zulfiqar, S., Warsi, M.F., Ejaz, S.R., Elnaggar, A.Y., et al., 2022. Wet-chemical synthesis of nanostructured Ce-doped mixed metal ferrites for the effective removal of azo dyes from industrial discharges. *Ceram. Int.*
- Kumar, P., Chand, P., 2022. Sm^{3+} - BiFeO_3 nano catalyst: A synergetic effect of Sm^{3+} on enhanced multiferroic properties and photocatalysis. *J. Alloys Compd.* 891, 161896.
- Li, S., Tang, Y., Wang, M., Kang, J., Jin, C., Liu, J., et al., 2021. $\text{NiO/g-C}_3\text{N}_4$ 2D/2D heterojunction catalyst as efficient peroxymonosulfate activators toward tetracycline degradation: characterization, performance and mechanism. *Journal of Alloys and Compounds* 880, 160547.
- Mansour, S.F., Ahmed, M.A., El-Dek, S.I., Abdo, M.A., Kora, H.H., 2017. Enhancement of the physical properties of novel $(1-x)\text{NiFe}_2\text{O}_4+(x)\text{Al}_2\text{O}_3$ nanocomposite. *Appl. Phys. A.* 123 (7), 1–11.
- Mansour, S.F., Abdo, M.A., Kzar, F.L., 2018a. Effect of Cr dopant on the structural, magnetic and dielectric properties of Cu-Zn nanoferrites. *J. Magn. Mater.* 465, 176–185.
- Mansour, S.F., Abdo, M.A., Alwan, S.M., 2018b. The role of Cr^{3+} ions substitution on structural, magnetic and dielectric modulus of manganese zinc nanoferrites. *Ceram. Int.* 44, 8035–8042.
- Mansour, S.F., Dawood, A., Abdo, M.A., 2019. Enhanced magnetic and dielectric properties of doped Co-Zn ferrite nanoparticles by virtue of Cr^{3+} role. *J. Mater. Sci.: Mater. Electron.* 30 (18), 17262–17275.
- Mansour, S.F., Al-Wafi, R., Abdo, M.A., 2020. Zn-Mg-La nanoferrites for storage and high frequency devices with augmenting the photocatalytic performance. *J. Alloys Compd.* 826, 154125.
- Mansour, S.F., Karamany, M.M., Al-Wafi, R., El-Dek, S.I., Almossalami, H.A., Abdo, M. A., 2021a. The effective role of diamagnetic Pb ions in tailoring the magnetic and dielectric properties of BiFeO_3 nanomultiferroic. *J. Mater. Sci.: Mater. Electron.* 32 (3), 3621–3637.
- Mansour, S.F., Al-Hazmi, F., AlHammad, M.S., Sadeq, M.S., Abdo, M.A., 2021b. Enhancing the magnetization, dielectric loss and photocatalytic activity of Co-Cu ferrite nanoparticles via the substitution of rare earth ions. *J. Mater. Res. Technol.* 15, 2543–2556.
- Mansour, S.F., Wageh, S., Al-Wafi, R., Abdo, M.A., 2021c. Enhanced magnetic, dielectric properties and photocatalytic activity of doped Mg-Zn ferrite nanoparticles by virtue of Sm^{3+} role. *J. Alloys Compd.* 856, 157437.
- Mansour, S.F., Zaher, Hadeer, Al-Wafi, Reem, Almossalami, Hossam A., Abdo, M.A., 2021d. Tuning of structural, magnetic and dielectric properties of $\text{M}_{0.45}\text{La}_{0.10}\text{Fe}_{2.45}\text{O}_4$; (M = Mn, Co, Cu, Mg and Zn) nanoparticles: effect of particle size and porosity. *J. Mater. Sci.: Mater. Electron.*, 1741–17458 <https://doi.org/10.1007/s10854-020-04942-y>.
- Meena, S., Anantharaju, K.S., Vidya, Y.S., Renuka, L., Uma, B., Sharma, S.C., More, S.S., 2021. Enhanced sunlight driven photocatalytic activity and electrochemical sensing properties of Ce-doped MnFe_2O_4 nano magnetic ferrites. *Ceram. Int.* 47 (10), 14760–14774.
- Mmelesi, O.K., Masunga, N., Kuvarega, A., Nkambule, T.T., Mamba, B.B., Kefeni, K.K., 2021. Cobalt ferrite nanoparticles and nanocomposites: Photocatalytic, antimicrobial activity and toxicity in water treatment. *Mater Sci Semicond.* 123, 105523.
- Naik, S.R., Salker, A.V., 2012. Change in the magnetostructural properties of rare earth doped cobalt ferrites relative to the magnetic anisotropy. *J. Mater. Chem.* 22 (6), 2740–2750.
- Padalia, D., Johri, U.C., Zaidi, M.G.H., 2016. Effect of cerium substitution on structural and magnetic properties of magnetite nanoparticles. *Mater. Chem. Phys.* 169, 89–95.
- Shakil, M., Inayat, U., Khalid, N.R., Tanveer, M., Gillani, S.S.A., Tariq, N.H., et al., 2022. Enhanced structural, optical, and photocatalytic activities of Cd-Co doped Zn ferrites for degrading methyl orange dye under irradiation by visible light. *J. Phys. Chem. Solids.* 161, 110419.
- Somanathan, T., Abilarasu, A., Jermy, B.R., Ravinayagam, V., Suresh, D., 2019. Microwave assisted green synthesis $\text{Ce}_{0.2}\text{Ni}_{0.8}\text{Fe}_2\text{O}_4$ nanoflakes using calotropis gigantean plant extract and its photocatalytic activity. *Ceram. Int.* 45 (14), 18091–18098.
- Thankachan, S., Jacob, B.P., Xavier, S., Mohammed, E.M., 2013. Effect of samarium substitution on structural and magnetic properties of magnesium ferrite nanoparticles. *J. Magn. Mater.* 348, 140–145.
- Vinsha, P.A., Vinsla, J.A., Madhavan, J., Devanesan, S., AlSalhi, M.S., Nicoletti, M., Xavier, B., 2022. Impact of dysprosium doped (Dy) zinc ferrite (ZnFe_2O_4) nanocrystals in photo-fenton exclusion of recalcitrant organic pollutant. *Environ. Res.* 203, 111913.
- Zhang, J., Yan, M., Sun, G., Li, X., Liu, K., 2021. Visible-light photo-Fenton catalytic MgFe_2O_4 spinel: Reaction sintering synthesis and DFT study. *J. Alloys Compd.* 889, 161673.